Fabrication of precise aperiodic multichannel fibre Bragg grating filters for spectral line suppression in hydrogenated standard telecommunications fibre

ADENOWO A. GBADEBO,[1,*] ELENA G. TURITSYNA,[1] AND JOHN A. R. WILLIAMS [1]

[1]*Aston Institute of Photonic Technologies , Aston University, Birmingham, B4 7ET, UK*
[*]*a.gbadebo@aston.ac.uk*

Abstract: We demonstrate the design and fabrication of multichannel Fibre Bragg gratings (FBGs) with aperiodic channel spacings. These will be suitable for the suppression of specific spectral lines such as OH emission lines in the Near InfraRed (NIR) which degrade ground based astronomical imaging. We discuss the design process used to meet a given specification and the fabrication challenges which can give rise to errors in the final manufactured device. We propose and demonstrate solutions to meet these challenges.

OCIS codes: (060.3738) Fiber Bragg gratings, photosensitivity; (350.1270) Astronomy and astrophysics.

References and links

1. S. Ellis and J. Bland-Hawthorn, "Speciality optical fibers for advanced astronomical instrumentation," SPIE Newsroom pp. 2–5 (2015).
2. K. A. Ennico, I. R. Parry, M. A. Kenworthy, R. S. Ellis, C. D. Mackay, M. G. Beckett, K. Glazebrook, J. Brinchmann, J. M. Pritchar, A. Aragon-Salamanca, K. Glazebrook, J. Brinchmann, J. M. Pritchard, S. R. Medlen, F. Piche, R. G. McMahon, and F. Cortecchia, "The Cambridge OH Suppression Instrument (COHSI): Status After First Commissioning Run," in "Astronomical Telescopes & Instrumentation," , vol. 3354 A. M. Fowler, ed. (1998), pp. 668–674.
3. S. C. Ellis and J. Bland-Hawthorn, "The case for OH suppression at near-infrared wavelengths," Mon. Not. R. Astron. Soc. **386**(1), 47–64 (2008).
4. J. Bland-Hawthorn, M. Englund, and G. Edvell, "New approach to atmospheric OH suppression using an aperiodic fibre Bragg grating." Opt. Express **12**(24), 5902–9 (2004).
5. T. Zhu, Y. Hu, P. Gatkine, S. Veilleux, J. Bland-Hawthorn, and M. Dagenais, "Arbitrary on-chip optical filter using complex waveguide Bragg gratings," Appl. Phys. Lett. **108**(10), 101104 (2016).
6. W. W. Morey, G. Meltz, and W. H. Glenn, "Fiber Optic Bragg Grating Sensors," in "OE/FIBERS '89," R. P. DePaula and E. Udd, eds. (International Society for Optics and Photonics, 1990), pp. 98–107.
7. G. Meltz, W. W. Morey, and W. H. Glenn, "Formation of Bragg gratings in optical fibers by a transverse holographic method," Opt. Lett. **14**(15), 823–825 (1989).
8. K. Hill, B. Malo, F. Bilodeau, and D. Johnson, "Photosensitivity in optical Fibres," Annu. Rev. Mater. Sci. **23**, 125–157 (1993).
9. M. J. Cole, T. Widdowson, and A. D. Ellis, "10cm chirped fibre Bragg grating for dispersion compensation at 10Gbit/s over 400 km," Electron. Lett. **31**(25), 2203–2204 (1995).
10. M. Cole, W. H. Loh, R. I. Laming, M. N. Zervas, and S. Barcelos, "Moving fiber/phase maskscanning beam technique for enhanced flexibility in producing fibre gratings with uniform phase mask," Electron. Lett. **31**(17), 1488–1490 (1995).
11. I. J. F. Brennan, D. LaBrake, G. A. Beauchesne, and R. P. Pepin, "Method for fabrication of in-line optical waveguide index grating of any length," Patent US5912999 (1999).
12. M. Durkin, M. Ibsen, M. Cole, and R. Laming, "1 m long continuously-written fibre Bragg gratings for combined second-and third-order dispersion compensation," Electron. Lett. **33**(22), 1891–1893 (1997).
13. Q. Zhang, D. A. Brown, L. Reinhart, T. F. Morse, J. Q. Wang, and G. Xiao, "Tuning Bragg wavelength by writing gratings on prestrained fibers," IEEE Photonics Technol. Lett. **6**(7), 839–841 (1994).
14. Y. Liu, J. Pan, and C. Gu, "Novel fiber Bragg grating fabrication method with high-precision phase control," Opt. Eng. **43**(8), 1916 (2004).
15. J. Skaar, L. Wang, and T. Erdogan, "On the synthesis of fiber Bragg gratings by layer peeling," IEEE J. Quantum Electron. **37**(2), 165–173 (2001).

16. A. Buryak, K. Kolossovski, and D. Y. Stepanov, "Improved multi channel grating design," Patent WO2003079083A1 (2003).
17. C. L. Liou, L. A. Wang, and M. C. Shih, "Characteristics of hydrogenated fiber Bragg gratings," Appl. Phys. A Mater. Sci. Process. **64**(2), 191–197 (1997).
18. A. A. Gbadebo, E. G. Turitsyna, and J. A. R. Williams, "Experimental Comparison of Differing Design Approaches for Multichannel Fibre Bragg Gratings," The European Conference on Lasers and Electro-Optics **854**, 12110 (2015).
19. A. Gbadebo, E. Turitsyna, and J. Williams, "Experimental Demonstration of Real-time correction of writing errors during Fibre-Bragg grating fabrication," in "Photonics and Fiber Technology 2016 (ACOFT, BGPP, NP)," vol. 3 (OSA, Washington, D.C., 2016), paper BTh1B.2.
20. S. Loranger and R. Kashyap, "Fiber Imperfections and their Impact on the Performance of Fiber Grating DFB Raman Lasers," in "Nonlinear Optics," (OSA, Washington, D.C., 2017), 1, paper NW4A.17.
21. H. Cao, J. Atai, J. Zuo, Y. Yu, A. Gbadebo, B. Xiong, J. Hou, P. Liang, Y. Gao, and X. Shu, "Simultaneous multichannel carrier-suppressed return-to-zero to non-return-to-zero format conversion using a fiber Bragg grating," Appl. Opt. **54**(20), 6344 (2015).
22. I. Bennion, J. Williams, and L. Zhang, "UV-written in-fibre Bragg gratings," Opt. Quantum Electron. **28**(2), 93–135 (1996).
23. H. Yin, A. Gbadebo, and E. G. Turitsyna, "Top-hat random fiber Bragg grating," Opt. Lett. **40**(15), 3592 (2015).
24. I. Petermann, B. Sahlgren, S. Helmfrid, A. T. Friberg, and P. Y. Fonjallaz, "Fabrication of advanced fiber Bragg gratings by use of sequential writing with a continuous-wave ultraviolet laser source.," Appl. Opt. **41**(6), 1051–1056 (2002).
25. A. Gbadebo, E. Turitsyna, J. Williams, and S. Turitsyn, "Fibre grating filters for suppression of near infrared OH emission lines," 39th European Conference and Exhibition on Optical Communication (ECOC 2013) **2013**, 852–854 (2013).
26. J. Skaar and O. Waagaard, "Design and characterization of finite-length fiber gratings," IEEE J. Quantum Electron. **39**(10), 1238–1245 (2003).
27. H. Cao, J. Atai, X. Shu, and G. Chen, "Direct design of high channel-count fiber Bragg grating filters with low index modulation." Opt. Express **20**(11), 12095–110 (2012).
28. A. V. Buryak, K. Y. Kolossovski, and D. Y. Stepanov, "Optimization of refractive index sampling for multichannel fiber Bragg gratings," IEEE J. Quantum Electron. **39**(1), 91–98 (2003).
29. E. G. Turitsyna, A. Gbadebo, and J. A. R. Williams, "A technique for mitigating the effect of the writing-beam profile on fibre Bragg grating fabrication," Opt. Express **23**(10), 12628–12635 (2015).
30. H. Li, M. Li, Y. Sheng, and J. E. Rothenberg, "Advances in the design and fabrication of high-channel-count fiber Bragg gratings," J. Light. Technol. **25**(9), 2739–2750 (2007).
31. J. Chen, T. Liu, and H. Jiang, "Optimal design of multichannel fiber Bragg grating filters using Pareto multi-objective optimization algorithm," Opt. Commun. **358**, 59–64 (2016).
32. B. Malo, J. Albert, K. Hill, F. Bilodeau, and D. Johnson, "Effective index drift from molecular hydrogen diffusion in hydrogen-loaded optical fibres and its effect on Bragg grating fabrication," Electron. Lett. **30**(5), 442–444 (1994).
33. P. Swart and A. Chtcherbakov, "Study of hydrogen diffusion in boron/germanium codoped optical fiber," J. Light. Technol. **20**(11), 1933–1941 (2002).
34. G. Brochu, S. LaRochelle, and N. Ayotte, "Dynamics of hydrogen diffusion as a key component of the photosensitivity response of hydrogen-loaded optical fibers," J. Light. Technol. **27**(15), 3123–3134 (2009).

1. Introduction

There is a demand for multichannel filters for OH emission filtering [1] of Near InfraRed (NIR) wavelengths collected from ground telescopes [2]. OH emission lines generated in the atmosphere make it challenging to observe distant red shifted galaxies. Several methods have been applied to suppress OH emissions including high dispersion masking, Rugate filters and holographic filters. Each of the methods has some major setbacks in achieving full suppression of the spectrum [3]. Bland-Hawthorn et al. (2004) introduced the application of FBGs to OH suppression [4], that enables NIR inspection from ground telescopes. Zhu et al. (2016) fabricated multichannel on-chip optical filter in complex waveguides with a plan to extend the channels from 20 to 100 [5].

Fibre Bragg gratings were identified as having application as multichannel filters, particularly for sensing, from the very beginnings of the development of the technology [6]. The availability of arbitrary profile FBGs was limited by the capability of early fabrication approaches [7, 8]. The development of gratings for the telecommunication industry [9] increased with the advent of refractive index apodisation and beam scanning [10, 11] which facilitated fabrication of long FBG [12] and the introduction of chirp [13]. These techniques also revealed the problem of inscription beam size on FBG fabrication [10]. Over the next decade there was a focus on

increasing the chirping and apodisation capabilities of grating fabrication [14–16].

The characteristics of fabricated gratings depend on the geometry, refractive index, presence of defects, fibre drawing process and hydrogen in the cladding and core of a fibre. They also depend on the nature of the ultraviolet (UV) radiation source that triggers the change in refractive index – the intensity and shape of the beam and the wavelength of the beam. When writing gratings it is challenging to estimate the final wavelength of the device due to the non-linear effects of the fibre photosensitivity, particularly if the fibre is "hydrogen loaded" to increase its photosensitivity [17]. The current state of the art of grating fabrication focuses on increased the fidelity between an expected design and the fabricated device [18] and on characterisation of the fibre and grating to enable fabrication of accurate complex arbitrary profile long gratings [19, 20]. Such gratings have tight constraints in terms of maximum allowed deviation from requirements with respect to wavelength and grating strength. In previous work, Cao et. al. [21] demonstrated the application of multichannel grating for conversion of signals from return to zero to non-return to zero where the tolerance of error in the grating's bandwidth is 32 pm.

Fabrication of multiple channels in a single grating inscription has the advantage of eliminating the need to splice multiple devices together and the subsequent losses induced. It requires the stripping of a smaller length of fibre helping to maintain structural integrity. Fabrication setups that can handle multichannel gratings must function continuously over a wide spectral range and be able to introduce apodisation and change of period along the grating length to achieve arbitrary profile gratings.

In this work we compare the difference between the measured fabricated grating spectral response and the expected spectral response in an application specific way. We have examined a range of applications that require very specific grating spectral and delay profiles [22, 23] including OH emission line suppression for astrophysics applications which we focus on here. This research attempts to underpin the sources for errors observed after fabricating multichannel gratings and establishes methods to mitigate such errors through the fabrication process.

2. Fabrication configuration

The designed gratings are fabricated with a setup that uses an acoustic optical modulator (AOM) to modulate a beam generated by a 100 mW, 244 nm frequency doubled argon ion laser. The beam is incident on a phase mask which is used to generate an interference pattern. The modulation is controlled by a software that converts the designed gratings' profiles to intensity levels similar to the work of Cole [10], Liu [14] and Petterman [24]. During the grating fabrication the fibre is placed within the interference pattern and scanned across the phase mask at a predetermined rate by a high precision linear motor stage. The beam is measured at the point of incidence on the fibre with a diameter of 270μm during fabrication. The diameter was maintained for all other fabricated gratings mentioned in this paper. All gratings are fabricated in standard telecommunications (SMF 28) fibre (except where otherwise specified) after been hydrogenated for 4 days at 100 bar and 80°C. Final profiles are measured after annealing in an oven at 80°C over 48 hours. All environmental factors are considered and monitored during fabrication to ensure similar conditions for all gratings. All gratings are measured with an optical spectrum analyser (OSA) pre-annealing and with a LUNA optical vector analyser post annealing.

3. Target spectrum design and observation of errors in fabrication

As a proof of concept, we consider a 5-channel grating with varying spectral spacing which has application in astrophysics [25]. The target spectrum was designed and converted to the complex coupling coefficient (CC) using the inverse layer peeling (LP) algorithm [26]. This resulted in the amplitude of the complex CC (D1) shown in Fig. 1(a) determined by the spectrum shown in Fig. 1(b).

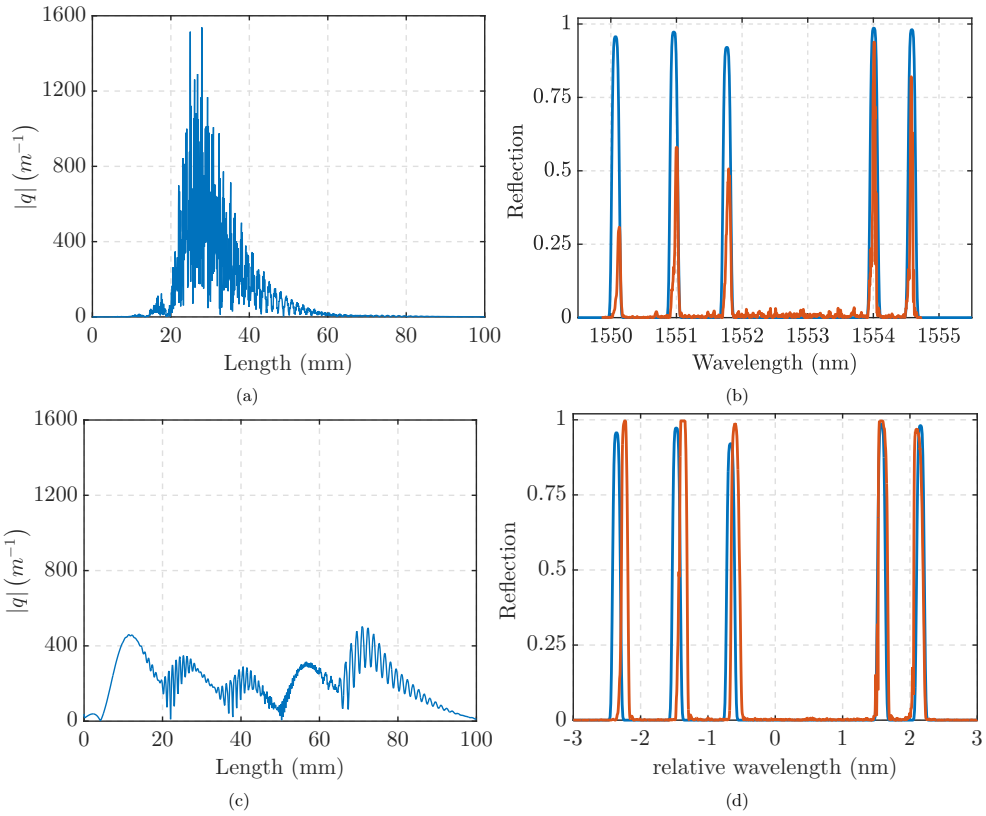

Fig. 1. Designed aperiodic multichannel grating (a) Amplitude of coupling coefficient (CC) (grating D1) (b) Comparison of the target spectrum (blue line) and fabricated (red line) reflection spectrum (C) Amplitude of spread coupling coefficient (CC)(grating D2), (d) target spectrum (blue line) and fabricated (red line) multichannel grating

The 5-channel multichannel grating is designed with each channel having a super-Gaussian shape. It was designed as described in Eq. (1):

$$|r(\lambda)| = \sqrt{R_j} \sum_{j=1}^{N} \exp\left(-\left(\frac{\lambda - \lambda_j}{b}\right)^4\right) \times \exp\left(i2\pi n_{\text{eff}}\left(\frac{1}{\lambda} - \frac{1}{\lambda_j}\right) d_j\right) \tag{1}$$

where N is the number of channels, $b = 0.15$ nm is the bandwidth of each channel, n_{eff} the effective refractive index, R_i is the desired reflectivity, λ_j (in nm) is the central wavelength, and d_{j} is a group delay parameter of the j-th channel. The central wavelength for each channel is shown in Table 1. The group delay parameter applies independent group delays to each channel, which directly maps to different locations in the physical domain [27, 28]. The channel group delay parameters used in each design are shown in Table 2 . Eq. (1) allows for independent control of the inter-channel spacing, strength and bandwidth.

Table 1. 5 OH emission line wavelengths and strengths to be suppressed

Wavelength (nm)	1550.086	1550.977	1551.787	1554.033	1554.614
Strength (dB)	-14	-16	-11	-19	-18

Table 2. Group delay parameter for each channel in each grating design

Grating design	Group delay parameters (mm)				
	d_1	d_2	d_3	d_4	d_5
D1	50	50	50	50	50
D2	10	25	40	55	70
D3	15	30	37.5	45	60
D4	17.5	17.5	17.5	42.5	42.5

Initial fabrication of the multichannel gratings revealed errors in the most important characteristics. These errors included channel strength reduction due to the beamwidth and/or insufficient photosensitivity, errors in the channel bandwidths, and inter-channel spacing errors. The most significant error was in channel strength which increased as the detuning of the grating from the central wavelength of the interference pattern increased. This was attributed to the beam size as described by Cole et. al. [10]. Gratings experience a washing out of its fringes as the wavelength of the channel written is detuned from the central wavelength. This affects any fabrication method that uses two beam interference to fabricate a grating. The beam size error can be mitigated by applying the algorithm described by Turitsyna et. al. [29]. Once this issue is mitigated the inter-channel spacing error and reduced channel strength due to the fibre photosensitivity became apparent, as can be seen in Fig. 1. This beam size mitigating algorithm was applied to all the gratings fabricated in this paper.

In Fig. 1(a) we show the design of a multichannel grating with a maximum coupling coefficient amplitude of $1600\,m^{-1}$. The design profile has high frequency components beyond what can be fabricated and requires a change in reflective index of 8.5×10^{-4}. Figure 1(a) shows the target and actual measured spectral response for this grating clearly showing the impact of the fabrication limitations.

These high frequency components of the grating profile can be reduced by changing the group delay parameter in Eq. (1), hence controlling the spacial overlap of the channels. This produces a new profile (D2) shown in Fig. 1(c) which was fabricated and shown in Fig. 1(d) (red line). This reduces the maximum refractive index change required to 2.1×10^{-4} without changing the grating target response as seen in Fig. 1(d) (blue line) [27, 30, 31].

4. Inter-channel spacing error in multichannel gratings

Shifts in channel wavelength have previously been observed to occur during fabrication [32] and been attributed to the effect of the diffusion of the hydrogen (or deuterium) used to increase fibre photosensitivity [33,34]. The channel locations are observed to experience a red shift immediately after fabrication followed later by a blue shift. The effect of this on inter-channel spacing for multichannel filters has not previously been reported. In the next section we investigate the effect of photosensitivity and environmental factors that determine the wavelength of a fabricated grating to determine their influence on the inter-channel spacing in multichannel gratings.

The drift in the central wavelength of channels in a multichannel fabricated is observed to be non-uniform across the fibre when writing into hydrogenated fibre. An error of about 50 pm is observed in the channel positions, which is significant for a channel that is only 150 pm wide. Such an error can be crucial when working with lasers and complex grating designs that require narrow spectra or have a low tolerance of variance. In order to track down the source of the error the conditions of writing the gratings are investigated.

Multiple single-channel 10 mm uniform gratings were used to observe the effects of strain, temperature, hydrogen left in fibre and refractive index change through a series of experiments. An increase in strain and temperature applied to the fibre during fabrication induced a reduction in red

shift of the channels. The increase was observed to be uniform across the fibre. This is attributed to faster out-diffusion of hydrogen from the fibre core. A constant strain and temperature on the fibre during fabrication was observed to have a negligible effect on the error in inter-channel spacing observed. On the other hand, the reduction in hydrogen content and change in refractive index could lead to the detected errors, since they both experience significant changes during the fabrication of multichannel gratings. This is because multichannel gratings (see Fig. 1) often have a complex fast varying coupling coefficient, and it takes prolonged periods of up to several hours to fabricate them.

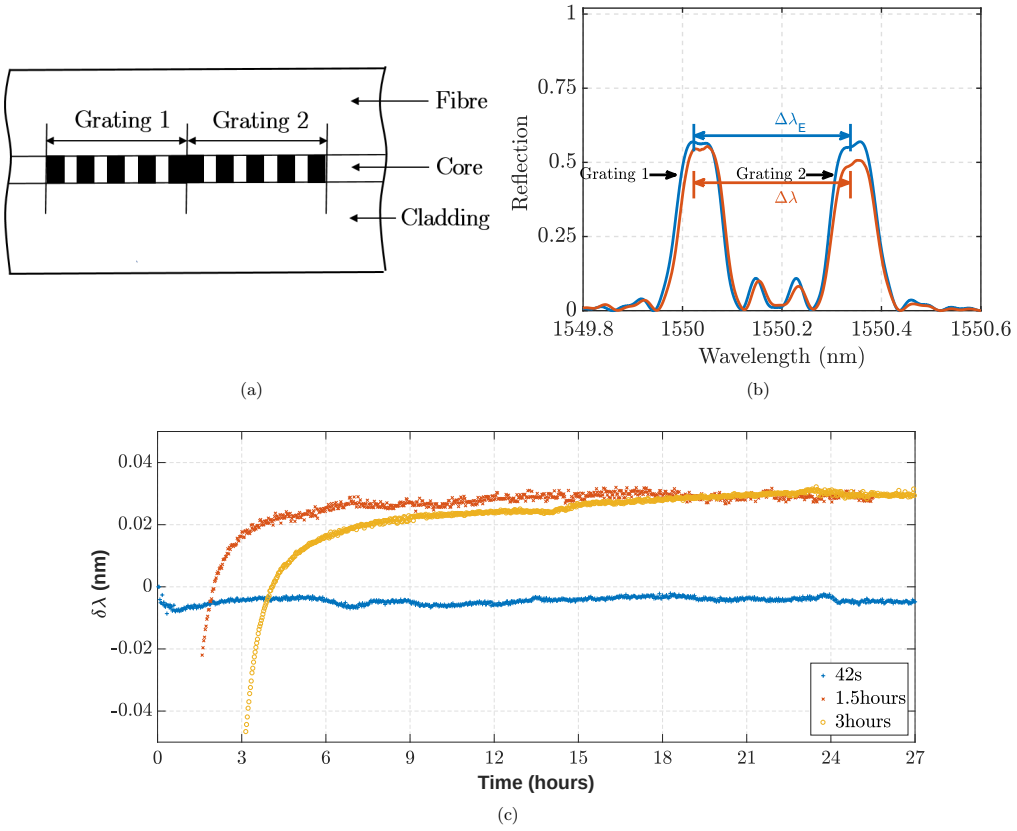

Fig. 2. (a) Schema of gratings positioned next to each other in the fibre (b) simulated(blue line) and fabricated (red line) reflection spectrum of two channels next to each other in the fibre (c) Deviation from expected inter-channel spaces, $\delta\lambda$, for gratings written at different times

The effect of hydrogen diffusion was observed by fabricating two gratings (with parameters as described in the previous paragraphs) next to each other (in the fibre as shown in Fig. 2(a)) but at different wavelengths (1550 nm and 1550.318 nm as shown in Fig. 2(b)) with varying delays between time of fabrication (42 s, 1.5 hours, 3 hours). This is shown in Fig. 2(c) which is a plot of the change in wavelength, $\delta\lambda$ and $\delta\lambda = \Delta\lambda - \Delta\lambda_E$ where $\Delta\lambda$ is the measured inter-channel spacing of the fabricated grating and $\Delta\lambda_E$ is the expected inter-channel spacing from the target spectrum. It (Fig. 2(c)) demonstrates the difference between the actual (311 pm, 348 pm and 348 pm after saturation) and the expected (318 pm) inter-channel spacing relative to the hydrogen content of the fibre. It can be seen from Fig. 2(c) that when the second channel is written 42 s after the first (blue line) the inter-channel spacing is 311 pm where the expected inter-channel spacing is 318 pm. When there is more delay between writing there is an inter-channel spacing

error that saturates at 30 pm. The time to saturation can be seen to increase as the time between writing increases.

The result of this study shows that the time required for writing multichannel gratings, hence the hydrogen left in the fibre, has a significant impact on the inter-channel spacing. It also suggests that reduction of channel overlap by tuning the group delay parameter needs to be optimised to achieve a balance between wavelength accuracy and channel strength.

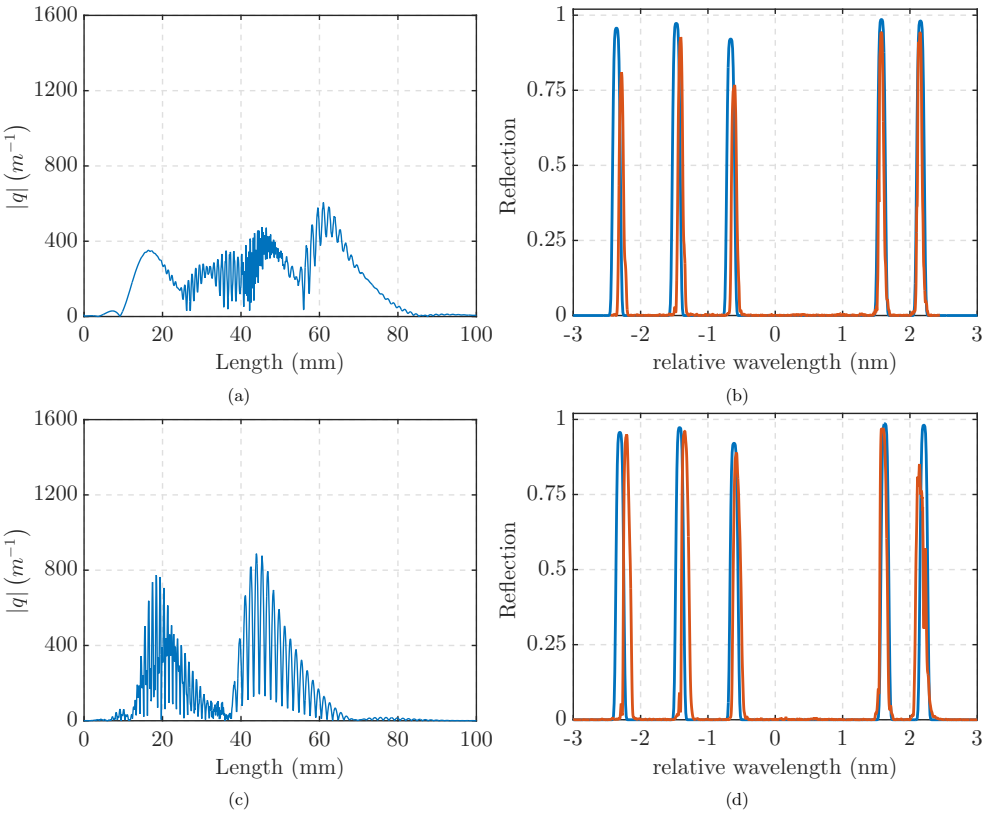

Fig. 3. Designed and fabricated 5-channel gratings (a) Amplitude of coupling coefficient (CC) (D3) (b) Comparison of the designed (blue line) and fabricated (red line) reflection spectrum for D3 (c) Amplitude of coupling coefficient (CC) (D4) (d) Comparison of the designed (blue line) and fabricated (red line) reflection spectrum for D4

5. Optimising the group delay parameter

In order to tackle the effect of hydrogen on grating D2 and reduce the fast varying components in D1 two other designs are considered as seen in Fig. 3(a) and 3(c). The group delay parameters, d_j (shown in Table 2), are redistributed such that D3 is as shown in Fig. 3(a) and D4 is as shown in Fig. 3(c).

There is a significant improvement in the match between the designed and fabricated grating when there is a partial overlap in channels. It is observed that these two designs (D3, D4) show similar improvements in the spectrum and are a better match to the design than the completely superimposed (D1) and completely spread coupling coefficient (CC) (D2) as shown in Fig. 3. The deviation of the all channels from expected locations, λ_{RMSD}, is calculated using the root mean square deviation (RMSD) of the errors.

The deviation of the strength V_{RMSD} from expected channel strength is calculated using the RMSD of the strength of the grating, V. V is calculated as shown in Eq. (2).

$$|q|_{\max} \propto V = \frac{\tanh^{-1}\left(\sqrt{R_{\max}}\right)}{L} \tag{2}$$

R_{max} is the maximum linear reflection strength of each channel. L is the length of the grating. The deviation of wavelength (blue triangle) and strength (red dots) of each design from the expected is presented in Fig. 4.

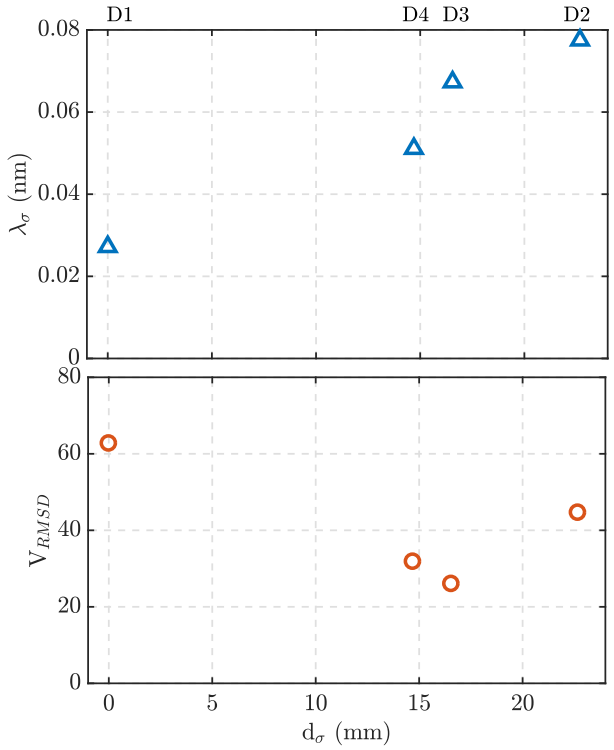

Fig. 4. The root mean square deviation (RMSD) of wavelength (blue triangle) and strength (red dots) of fabricated channels from expected for each design

Figure 4 shows that the strength deviation is highest when the standard deviation of the group delay parameter, d_σ, is 0 and it reduces with an increase in d_σ. It can also be seen that the strength error in D2 is high, breaking the trend observed in the previous designs, this is because the fabricated grating channels are stronger than the target spectrum. It (Fig. 4) shows that the wavelength deviation has the inverse relationship with deviation increasing as d_σ increases. The result shown in Fig. 3 and Fig. 4 implies that a trade off between wavelength and strength deviation of a grating design is important for when designing a multi-channel grating.

This trade-off is application specific, D4 is the design of choice for an application in signal conversion [21] from return to zero to non-return to zero as the wavelength RMSD error is around 50 pm. D3 on the other hand is more appropriate for OH emission line filtering as the channel strength is more critical in this application. This is because the channels are designed to be significantly wider than the spectral lines being filtered.

6. Conclusion

We have established a relationship between hydrogen content and errors observed in multichannel gratings. We have also shown that the error can be minimized by optimising the initial grating design. We are able to minimise errors by a factor of two. We have observed that inter-channel spacing and channel strength errors are introduced into the fabricated grating when the fibre hydrogenation or the maximum amplitude of the coupling coefficient (CC) is not considered during design. Inter-channel spacing errors are observed to increase as the physical channel separation increases across the fibre. We are undertaking further work on estimating and applying the rate of flow (diffusion and infusion) of hydrogen in fibre to compensate for errors introduced when writing a multi-channel grating.